Journal of Mathematical Biology manuscript No.
(will be inserted by the editor)

Numerical Bifurcation Analysis of Delay Differential Equations Arising from Physiological Modeling

K. Engelborghs[1], V. Lemaire[2], J. Bélair[3], D. Roose[1]

[1] Department of Computer Science, Katholieke Universiteit Leuven, Belgium, e-mail: {Koen.Engelborghs,Dirk.roose}@cs.kuleuven.ac.be

[2] Département de Physique, Université de Montréal, Succursale Centre-Ville, C.P. 6128, H3C 3J7, Montréal, Québec, Canada and Centre de Recherches Mathématiques, Université de Montréal, e-mail: lemaire@crm.umontreal.ca

[3] Département de Mathématiques et de Statistique, Université de Montréal, Institut de Génie Biomédical, Université de Montréal, Centre for Nonlinear Dynamics in Physiology and Medicine, McGill University, Montreal and Centre de Recherches Mathématiques, Université de Montréal.

Received: date / Revised version: date

Abstract This paper has a dual purpose. First, we describe numerical methods for continuation and bifurcation analysis of steady state solutions and periodic solutions of systems of delay differential equations with an arbitrary number of fixed, discrete delays. Second, we demonstrate how these methods can be used to obtain insight into complex biological regulatory systems in which interactions occur with time delays: for this, we consider a system of two equations for the plasma glucose and insulin concentrations in a diabetic patient subject to a system of external assistance. The model has two delays: the technological delay of the external system, and the physiological delay of the patient's liver. We compute stability of the steady state solution as a function of two parameters, compare with analytical results and compute several branches of periodic solutions and their stability. These numerical results allow to infer two categories of diabetic patients for which the external system has different efficiency.

Key words delay differential equations – bifurcation analysis – numerical methods – physiological modeling

1 Introduction

Dynamical systems with time delays have been studied for more than two centuries, dating back to Euler, but most progress has occured in the twentieth century, with the significant contributions of Lotka [11] and Volterra [26]. Although there is now a substantial body of theory available, the global knowledge of delay equations has not been widely exploited by the scientific community. This is somewhat changing, nowadays, with a rapidly growing use of systems with delays in applied sciences, most notably mathematical biology and engineering. The main advantage of explicitly incorporating time delays in modeling equations is to recognize the reality of non-instantaneous interactions.

It is often difficult, if not impossible, to study analytically the behaviour of models from applied sciences; instead one has to turn to numerical calculations. In this article, we present a combination of numerical methods based upon continuation schemes, through which we can compute and analyze fixed points, periodic solutions and their stability for a system containing an arbitrary number of constant delays. By doing so we can compute bifurcation diagrams to reveal the branching behaviour of the system. Several such computational programs exist for systems of ordinary differential equations, for example Auto97 [2], but, until recently, not for systems of delay equations. The functionality that we present here is implemented in the Matlab package DDE-BIFTOOL which is freely available for scientific use. The manual [3] contains directions on how to obtain the package.

The numerical algorithms have previously been presented in [14] and [5]. Our aim here is to present them in a coherent framework together with their application on a real-life example taken from human physiology and medicine. This example is drawn from modeling studies on the dynamics of a physiological system whose aim is to regulate the glucose quantity in the human body. In this model, we are dealing with a system with delays via which we can study the interaction between the internal glucose-regulation system in a diabetic patient and a system of external assistance.

The numerical analysis of this model clearly highlights the possibilities of the numerical methods. Furthermore, we obtain some new results for a physiological problem relating to the regulation of glucose. In section 2 we derive the modeling equations. In section 3 we briefly discuss the most relevant properties of delay equations and introduce some notation. In section 4 we discuss numerical methods for analyzing steady state solutions, apply them on our model and compare with analytical results. In section 5 we discuss and apply

methods for computing branches of periodic solutions and their stability. We briefly discuss medical implications of our results in section 6 and conclude in section 7. The sections on the methods for analysis of delay equations (sections 3, 4 and 5) can be read independently of the sections on physiological modeling (sections 2 and 6).

2 Derivation of the Modeling Equations

The blood-glucose concentration is controlled by a regulation system which is part of the endocrine system. This system is sometimes faulty, however, and diabetes is one of its major dysfunctions.

Medical research offers many therapeutic treatments to try to overcome this disease. One of the most promising recent research directions regarding certain types of patients is to try to construct an external system for regularizing the blood-glucose quantity, which would assist or even replace the defaulting internal system of the patient [20,18]. External systems are simply control systems in feedback form for the glucose quantity.

Unfortunately, designing and implementing such an external system gives rise to many problems, both with respect to its practical construction and its actual clinical efficiency. Most doctors believe it is only a question of technological or bio-technological aspects [10, 21], and when these are improved sufficiently, the system should work properly. However, we will argue that some of the encountered problems, like for example the instabilities of the glucose concentration one can observe during the glucose clamp presented in [9], are of a completely different nature: these problems are of dynamical nature. Indeed, each time the device measures glycaemia and then reacts accordingly, there is a delay introduced in the control loop [9,21,23,10]. The presence of this inherent delay perturbs the entire system and leads to instabilities in the glucose concentration — and this can be harmful for the patient [24].

Our model is derived from an existing model for internal glucose regulation (cf. Sturis *et al.* [25]) which was originally designed to show that a pancreatic pacemaker is not necessary to explain the existence of oscillations in the glucose concentration observed in healthy subjects. It shows that the structure of the autonomous regulatory system (feedback between glucose and insulin) is sufficient to induce these oscillations. Here, we modify the model to study the interactions between the internal regulation of glucose of a patient, and an external system of insulin administration. Our version of the model

consists of two compartments: the plasmatic insulin and the plasmatic glucose. Its mathematical expression simply represents fluid exchanges between the compartments and the external medium,

$$\begin{cases} \dot{I} = f_1(G) - \frac{I}{t_1} \\ \dot{G} = Eg + f_5(I(t-\tau_2)) - (f_2(G) + f_3(G) \cdot f_4(I)) \ . \end{cases} \tag{1}$$

Changes from the model of [25] are a decrease in the number of physiological compartments (one insulin compartment instead of two) and the incorporation of a discrete time delay to account for the delayed production of glucose by the liver stimulated by the presence of insulin. These changes do not impair the predictive power of the model, since the additional compartment used by Sturis *et al.* represented, indirectly, the delayed interaction between insulin concentration and glucose production.

In equation (1), I represents the insulin quantity (mU) and G the glucose quantity (mg). The function $f_1(G)$ represents the pancreatic insulin supply and I/t_1 is the degradation rate of the insulin by the body. Eg represents the glucose quantity supplied by the external medium, through injection at a constant rate (this term corresponds to food intake). The function $f_5(I)$ represents the production of hepatic glucose (the liver has a non negligible reaction time (delay) τ_2), whereas $f_2(G) + f_3(G) \cdot f_4(I)$ represents the utilization of glucose by certain tissues.

The precise form of the functions f_1, ..., f_5 (taken from [25]) depends essentially on experimental data:

$$\begin{cases} f_1(G) = \frac{209}{1+\mathrm{e}^{-\frac{G}{300\ V_3}+6.6}} \ , \quad f_2(G) = 72\ (1-\mathrm{e}^{-\frac{G}{144\ V_3}}) \ , \\ f_3(G) = \frac{0.01\ G}{V_3} \ , \quad f_4(I) = \frac{90}{1+\mathrm{e}^{-1.772\times\log\left(\frac{I}{V_1}\right)+7.76}} + 4 \ , \\ f_5(I) = \frac{180}{1+\mathrm{e}^{\frac{0.29\ I}{V_1}-7.5}} \ . \end{cases} \tag{2}$$

There are five parameters: V_1 is the volume of the insulin compartment, t_1 is the degradation characteristic time for the insulin (equivalent to a half-life excretion period), V_3 is the volume of the glucose compartment and Eg and τ_2 are as described above. The reference values of the parameters are:

$$V_1 = 3\,\mathrm{l},\ t_1 = 6\,\mathrm{min},\ V_3 = 10\,\mathrm{l},\ Eg = 180\,\mathrm{mg/min} \text{ and } \tau_2 = 50\,\mathrm{min}.$$

System (1) only represents the internal system of a normal person. To take into account the external system that interacts with the internal system in case of a diabetic patient, we need to modify

the expression for the function f_1 representing the pancreatic insulin production. Diabetes implies a decrease in the internal insulin production, hence this process is well described by the term $\alpha\ f_1(G)$, where α is a real number in [0,1]. In other words, α represents the affection degree of the patient: the smaller α is, the more affected the patient is.

The hypoglycaemic action of the external system imitates the behaviour of the internal system. Therefore, we will represent it by the term $(1-\alpha)\, f_1(G(t-\tau_1))$. The parameter τ_1 corresponds to the reaction time of the external system; it is precisely the delay we have mentioned at the beginning of the section. The term $\alpha f_1(G(t))$ represents the fraction α of insulin delivered by the pancreas of a normal subject into the circulation to maintain blood sugar at its physiological level. The term $(1-\alpha)f_1(G(t-\tau))$ stands for the remaining insulin, in the case of a diabetic subject, injected by the external system in response to glycaemia measured a time τ_1 in the past: τ_1 is therefore the time taken by the system to complete a single processing cycle. This representation implies that glucose is measured (and insulin injected) continuously by the external system: in practice, such is not generally the case, as external systems measure glucose in a discrete, but frequent, fashion. The continuous measurement is an idealization of this process. However, some closed-loop control systems are now able to measure and adjust the control variables continuously.

It may seem odd, and possibly incorrect, to use the same function f_1 to represent both the pancreatic insulin production and the exogenous insulin supply, since these two processes are independent, the first one being a biological phenomenon and the second one an artificial phenomenon. But this is merely a mathematical simplification that allows to study the effect of the delay τ_1 in isolation. If our goal had been to model a realistic external system, a more appropriate model of the interaction between external and internal systems would have been necessary, but one would still be left with the inherent delay effect. Most external systems used today are based on an internal algorithm that requires not only the input of the ambient glycaemia but the previous 5-minute trend in blood glucose levels. The algorithm uses the history of the glucose concentration to determine whether the blood glucose level is rising or falling, and produces a dosage of insulin that the patient should receive [1]. Unfortunately, these approaches remain largely ineffective [9].

The final expression of our model is thus,

$$\begin{cases} \dot{I} = \alpha \cdot f_1(G) - \frac{I}{t_1} + (1-\alpha) \cdot f_1(G(t-\tau_1)) \\ \dot{G} = Eg + f_5(I(t-\tau_2)) - (f_2(G) + f_3(G) \cdot f_4(I)) \ . \end{cases} \tag{3}$$

In order to determine which parameters we shall vary to study the dynamics of the system, we first make a distinction between two categories of parameters: we have the internal parameters V_1, t_1, V_3, τ_2 and α which depend on the characteristics of each individual, and we have the external parameters τ_1 and Eg which can be modulated as the operator wishes.

Some internal parameters, i.e. V_1, t_1 and V_3, do not vary too much from one individual to another while α, and to a less extent, τ_2 do. In as much as we are interested in showing the effect of the reaction time of the external system, it is important to observe the evolution of solutions as τ_1 varies. It is also important to consider the patient's state, i.e. the changes in the value of the parameter α. Finally, it could be interesting to study several cases for different values of Eg and τ_2.

It should be emphasized that the purpose of our model is not to predict the exact time course of glucose and insulin in diabetic patients submitted to a system of external assistance, but rather to show that unexpected instabilities in the glucose concentration may occur naturally due to inherent delayed interactions introduced in the feedback loops.

3 Delay equations

In this paper we consider delay equations of the form

$$\dot{x}(t) = f(x(t), x(t-\tau_1), \ldots, x(t-\tau_m), \eta) \tag{4}$$

where $x(t) \in \mathbb{R}^n$, $f : \mathbb{R}^{n\times(m+1)} \times \mathbb{R}^k \to \mathbb{R}^n$ and $\eta \in \mathbb{R}^k$.

Due to the dependency on the past, a solution profile is not uniquely defined by the value of $x(t)$ at some fixed time t, instead one has to specify an initial solution segment over an interval of length τ where $\tau = \max_{i=1\ldots m}\{\tau_i\}$. The initial function segment belongs to $C = C([-\tau, 0], \mathbb{R}^n)$, the infinite-dimensional function space of continuous function segments mapping the delay interval $[-\tau, 0]$ into $\mathbb{R}^n$. Similarly, after integrating (4) over some time t, the function segment $x_t \in C$, with $x_t(\theta) = x(t-\theta)$, $\theta \in [-\tau, 0]$ comprises the state of the system which uniquely determines the rest of its future. Hence delay equations define infinite-dimensional systems. As a consequence, a scalar autonomous delay equation, unlike a scalar ordinary differential equation, can exhibit periodic, quasi-periodic and even chaotic behaviour.

We call $\mathcal{S}_f(t; x_0)$ the (nonlinear) solution operator which maps the initial function segment x_0 onto its image under integration of

(4) over time t, that is $\mathcal{S}_f(t;x_0) = x_t$. The delay equation (4) can (somewhat abstractly) be rewritten as defining a non-delayed flow in C, i.e.,

$$\dot{\phi} = \mathcal{A}\phi,\ \phi \in \mathcal{D}(\mathcal{A}), \tag{5}$$

where $\mathcal{A}$ is the infinitesimal generator of the semigroup of solution operators $\mathcal{S}_f(t)$ of (4), defined by

$$(\mathcal{A}\phi)(\theta) = \frac{d\phi(\theta)}{d\theta},\ -\tau \leq \theta \leq 0,$$

with domain

$$\mathcal{D}(\mathcal{A}) = \{\phi \in C : \dot{\phi} \in C, \dot{\phi}(0) = f(\phi(0), \phi(-\tau_1), \ldots, \phi(-\tau_m), \eta)\},$$

see [8,7]. As will be shown further, this form allows to extend traditional techniques for non-delayed differential equations to (5), provided one works in a functional analysis setting.

4 Steady State Analysis

A constant solution or steady state solution $x(t) \equiv x^* \in \mathbb{R}^n$ of (4) can be found as a solution of the nonlinear system

$$f(x^*, x^*, \ldots, x^*, \eta) = 0. \tag{6}$$

Although x^* does not depend on the values of the delays, the stability of x^* under (4) does depend on the value of each delay. When linearizing (4) around x^* one obtains a linear delay differential equation, called the variational equation, of the form

$$\dot{y}(t) = A_0(x^*, \eta)y(t) + \sum_{i=1}^{m} A_i(x^*, \eta)y(t - \tau_i), \tag{7}$$

where, using $f \equiv f(x^0, x^1, \ldots, x^m, \eta)$,

$$A_i(x^*, \eta) = \frac{\partial f}{\partial x^i}(x^*, x^*, \ldots, x^*, \eta),\ i = 0, \ldots, m.$$

When filling in the sample solution $v\mathrm{e}^{\lambda t}$ one obtains,

$$\begin{cases} (\lambda I - A_0(x^*, \eta) + \sum_{i=1}^{m} A_i(x^*, \eta)\mathrm{e}^{-\tau_i \lambda})v = 0, \\ \|v\| = 1, \end{cases} \tag{8}$$

i.e. a nonlinear eigenvalue problem with characteristic matrix

$$\Delta(\lambda) = \lambda I - A_0(x^*, \eta) + \sum_{i=1}^{m} A_i(x^*, \eta)\mathrm{e}^{-\tau_i \lambda}.$$

Equation (8) is usually rewritten in the form of a characteristic equation

$$\det(\Delta(\lambda)) = 0. \tag{9}$$

Equation (9) has an infinite number of roots λ that determine the stability of x^* in the usual way. That is, the steady state solution x^* is asymptotically stable provided all the roots of (9) have negative real parts. It is unstable if there exists a root with positive real part. When following a branch of steady state solutions as a function of a physical parameter η, a bifurcation occurs when an eigenvalue crosses the imaginary axis, i.e., $\lambda = 0$ or $\lambda = \mathrm{i}\omega$, $\omega \neq 0$. In the latter case, a Hopf bifurcation occurs, at which a branch of periodic solution emanates.

4.1 Numerical Methods

As discussed above, a steady state solution x^* is independent of the delays. Thus its branching behaviour can be found from a corresponding system of ordinary differential equations by putting all delays to zero and using a standard package for bifurcation analysis of ordinary differential equations [2]. On the other hand, stability analysis of steady state solutions is drastically different. Most existing studies tackle this problem analytically.

In order to determine numerically and efficiently the stability of a steady state solution, one needs a method which automatically selects and computes the rightmost (i.e. stability determining) roots of (9). Many numerical methods have been developed to compute selected eigenvalues of large eigenvalue and generalized eigenvalue problems, e.g. subspace iteration, Arnoldi, Jacobi-Davidson method, rational Krylov methods, see [22]. Most of these methods compute the dominant eigenvalues (i.e. largest in modulus), but can be combined with a suitable transformation (shift-invert, Cayley transformation) to compute the rightmost eigenvalues [17]. However none of these methods can be applied directly to (8) because they are based on the construction of bases of subspaces spanned by sets of eigenvectors v. For (8) this approach is no longer applicable. Indeed, if one considers, e.g., a scalar delay equation, then, the eigenvalue problem (8) will generally still have an infinite number of eigenvalues λ but all (scalar) eigenvectors v can be scaled to 1 and the concept of an eigenvector loses its meaning.

Only if the problem is considered to define a flow in its proper state space one can find a normal, albeit infinite-dimensional eigenvalue problem.

The eigenvalues of the infinitesimal generator $\mathcal{A}$ of the variational equation (7) equal the solutions of the characteristic equation. During computations we need to discretize the linear, unbounded operator $\mathcal{A}$ and to approximate it by a high-dimensional matrix $J \in \mathbb{R}^{N\times N}$, $N \gg 1$. J is a sparse matrix whose structure and sparseness depend on the number and the relative position of the delays.

The linear time integration operators $\mathcal{S}(t)$ of (7) are compact when $t \geq \tau$ and their eigenvalues are exponential transformations of the eigenvalues of $\mathcal{A}$, i.e. they are given by

$$\mu = \exp(\lambda t), \tag{10}$$

where λ is an eigenvalue of the characteristic equation (8) (plus possibly zero [7]). Discretizing $\mathcal{S}(t)$ leads to a high-dimensional dense matrix $M(t)$. The rightmost eigenvalues of (8) are, through the exponential transform (10), mapped to the dominant eigenvalues of $\mathcal{S}(t)$. Computing the dominant eigenvalues of a large matrix using only matrix-vector products is computationally easier than computing the rightmost eigenvalues and can be done using subspace iteration with projection, which is a well understood and robust numerical method. The efficiency of the procedure can be increased by using a Newton procedure on the characteristic equation as soon as good starting values for the eigenvalues are available. The modes thus found are then locked in subsequent subspace iterations. This approach is described in [5].

When following a branch of steady state solutions as a function of a parameter $\eta \in \mathbb{R}$, the previous algorithm can be used to monitor the stability along the branch and detect bifurcations. When an eigenvalue crosses the imaginary axis a bifurcation occurs. Once detected, a bifurcation can easily be computed and followed in two-parameter space [15,3].

4.2 Analytical Methods

Although the emphasis of this paper is on numerical methods for general systems of delay equations of the form (4), some results for system (3) can also be obtained using analytical methods. In this section we discuss these analytical results to compare with our numerical results. For a more general discussion of such methods, see for example [7].

We can show that system (3) has a *unique* steady state $x^* = (I^*, G^*)$ which is the solution of

$$\begin{cases} f_1(G^*) - I^*/t_1 = 0 \\ Eg + f_5(I^*) - f_2(G^*) - f_3(G^*) \cdot f_4(I^*) = 0 \ . \end{cases} \tag{11}$$

Note that G^* and I^* are independent of τ_1 and α. This property is interesting because it significantly simplifies the derivations presented in this section, and motivated some assumptions we introduced in the construction of the model.

Linearization of (3) around x^* yields the variational equations (7) where

$$y(t) = (i(t), g(t)) \ ,$$

$$A_0(x^*, \eta) = \begin{bmatrix} -1/t_1 & \alpha \cdot f_1'(G^*) \\ -f_3(G^*) \cdot f_4'(I^*) & -f_2'(G^*) - f_3'(G^*) \cdot f_4(I^*) \end{bmatrix} \ ,$$

$$A_1(x^*, \eta) = \begin{bmatrix} 0 & (1-\alpha) \cdot f_1'(G^*) \\ 0 & 0 \end{bmatrix} \text{ and } A_2(x^*, \eta) = \begin{bmatrix} 0 & 0 \\ f_5'(I^*) & 0 \end{bmatrix} \ ,$$

using $\eta = (V_1, t_1, V_3, \tau_2, Eg, \alpha, \tau_1) \in \mathbb{R}^7$ and f_i' for the derivative of f_i, $i = 1, \ldots, 5$.

The characteristic equation, given by equation (9), can now be written as

$$\lambda^2 + a\lambda + b + c \cdot \mathrm{e}^{-\lambda(\tau_1+\tau_2)} + d \cdot \mathrm{e}^{-\lambda\tau_1} + e \cdot \mathrm{e}^{-\lambda\tau_2} = 0 \ , \tag{12}$$

where

$$\begin{cases} a = 1/t_1 + f_2'(G^*) + f_3'(G^*) \cdot f_4(I^*) \ , \\ b = 1/t_1 \cdot (f_2'(G^*) + f_3'(G^*) \cdot f_4(I^*)) + \alpha \cdot f_1'(G^*) \cdot f_3(G^*) \cdot f_4'(I^*) \ , \\ c = -(1-\alpha) \cdot f_1'(G^*) \cdot f_5'(I^*) \ , \\ d = (1-\alpha) \cdot f_1'(G^*) \cdot f_3(G^*) \cdot f_4'(I^*) \ , \\ e = -\alpha \cdot f_1'(G^*) \cdot f_5'(I^*) \ . \end{cases}$$

Because f_1, ..., f_4 are monotonically increasing functions and f_5 is monotonically decreasing, it is easy to check that all these parameters are positive.

The fixed point (G^*, I^*) loses stability as the real part of a solution λ of equation (12) becomes positive. Hence the boundary of the stability zones (where $\lambda = \mathrm{i}\omega$, $\omega \in \mathbb{R}$) is determined by

$$\frac{-\omega^2 + a\mathrm{i}\omega + b + e \cdot \mathrm{e}^{-\mathrm{i}\omega\tau_2}}{-d - c \cdot \mathrm{e}^{-\mathrm{i}\omega\tau_2}} = \mathrm{e}^{-\mathrm{i}\omega\tau_1} \tag{13}$$

where $\omega \geq 0$ (the case "$\omega \leq 0$" corresponds to the complex conjugate).

The geometry of stability changes thus involves the intersection of two curves. One is the unit circle

$$\mathrm{e}^{-\mathrm{i}\omega\tau_1}$$

that is covered repeatedly as $\omega\tau_1$ increases from zero to infinity. The other curve is the *ratio curve* (as N. MacDonald calls it in [16]),

$$\frac{d\omega^2 - bd - ce - (de + c(b-\omega^2)) \cdot \cos\omega\tau_2 + ac\omega \sin\omega\tau_2}{c^2 + d^2 + 2cd\cos\omega\tau_2} + \mathrm{i}\,\frac{-ad\omega + (de - c(b-\omega^2)) \cdot \sin\omega\tau_2 - ac\omega\cos\omega\tau_2}{c^2 + d^2 + 2cd\cos\omega\tau_2},$$

that is covered only once as ω runs from zero to infinity. This last curve starts at the real point $-(b+e)/(c+d)$ for $\omega = 0$, and tends to infinity as $\omega \to +\infty$, making a spiral around the point $-(b+e)/(c+d)$. Of course, the spiral's form changes depending on the parameter values and, the number of intersection points with the unit circle may vary consequently.

Let us write the ratio curve as a complex-valued function $R_c(\omega, \alpha)$ of ω and α. Solutions of equation (13) satisfy

$$R_c(\omega,\alpha)\,\overline{R_c(\omega,\alpha)} = 1\ . \tag{14}$$

For each α, $0 \le \alpha \le 1$, we consider, whenever they exist, solutions ω_j, $j \in \mathbb{N}$, to the last equation (14) which are real and positive. With this notation, equation (14) becomes

$$\begin{cases} \mathfrak{Re}[R_c(\omega_j,\alpha)] = \cos(\omega_j\tau_{1,j}) \\ \mathfrak{Im}[R_c(\omega_j,\alpha)] = -\sin(\omega_j\tau_{1,j})\ . \end{cases} \tag{15}$$

Now, for every ω_j, let $\tau^0_{1,j}$ denote the solution of system (15) such that $0 \le \tau^0_{1,j} \le 2\pi/\omega_j$. For all k in $\mathbb{N}$, $\tau^k_{1,j} = \tau^0_{1,j} + 2k\pi/\omega_j$ is also a solution of system (15). Hence, for each couple $(\tau^k_{1,j}, \alpha)$, $k = 0, 1, 2, \ldots$ there is a pair of conjugate complex eigenvalues $\lambda = \pm\mathrm{i}\omega_j$ that are solutions of equation (9).

The set of points $(\tau^k_{1,j}, \alpha)$, for all j describes several curves in parameter space – depicted in figure 1. Denote these curves by $\mathcal{C}^k$. When the pair of parameters (τ_1, α) crosses a curve C^k, the sign of the real part of an eigenvalue changes sign and there can be a change of stability of the stationary state. The sign of the quantities

$$\mathrm{d}^k_{\tau_1} = \left.\frac{\partial\Big(\mathfrak{Re}[\lambda(\eta)]\Big)}{\partial\tau_1}\right|_{(\tau_1,\alpha)\in\mathcal{C}^k} \quad \text{and} \quad \mathrm{d}^k_{\alpha} = \left.\frac{\partial\Big(\mathfrak{Re}[\lambda(\eta)]\Big)}{\partial\alpha}\right|_{(\tau_1,\alpha)\in\mathcal{C}^k} \tag{16}$$

indicates the direction of change of the real part of the eigenvalue on the imaginary axis. If $\mathrm{d}^k_{\tau_1} \neq 0$ or $\mathrm{d}^k_{\alpha} \neq 0$, a Hopf bifurcation occurs at $\eta \in \mathcal{C}^k$, provided that either (i) all other eigenvalues of system (7) have nonzero real parts [19], or (ii) a non-resonance condition holds for the different pairs of purely imaginary eigenvalues.

4.3 Results

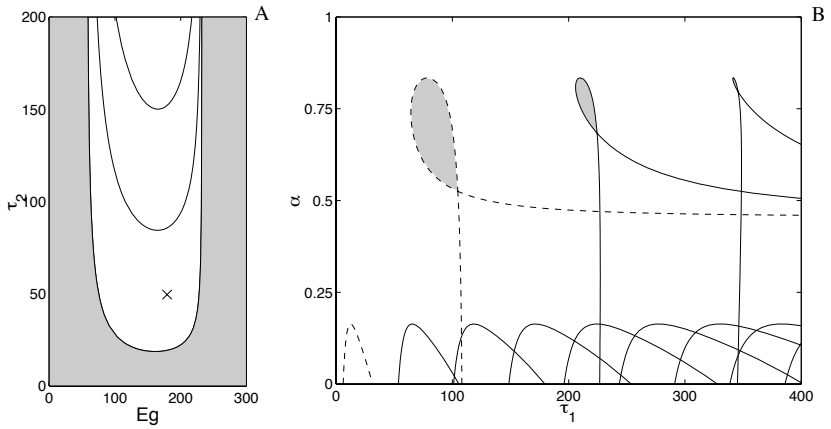

Fig. 1 Stability diagrams: Hopf curves and regions of local stability of the steady state solution. Left: Stability diagram for "healthy people" (1) in the plane (Eg, τ_2). Right: Curves of Hopf points of system (3) in the (τ_1, α)-plane for $Eg = 180$ and $\tau_2 = 50$.

Using the analytical methods of section 4.2, we determined the curves $\mathcal{C}^k$ shown in figure 1. Shadowed zones indicate stable stationary solutions. As indicated by a cross in figure 1-A, we have chosen $Eg = 180$ and $\tau_2 = 50$ to generate figure 1-B. We can see in figure 1-A that for these values of the parameters the stationary solution of system (1) is unstable. Thus, the stationary solution of system (3) is unstable for $\alpha = 1$ or $\tau_1 = 0$ (systems (1) and (3) are then equivalent), and (by continuity) for the neighbouring points in the (τ_1, α)-plane, see figure 1-B. The two parts of the dashed curve $\mathcal{C}^0$ in figure 1-B consist of points of type $(\tau^0_{1,j}, \alpha)$; the solid curves similar to the dashed ones but shifted to the right consist of points of type $(\tau^k_{1,j}, \alpha)$, $k \geq 1$ (i.e. $\mathcal{C}^1$, $\mathcal{C}^2$, ...).

Numerical bifurcation analysis commonly proceeds in a step-by-step fashion. Starting from a steady state solution for some given

fixed parameter values, a branch of steady state solutions is computed as a function of a single parameter. Computing and monitoring the stability along the branch allows to detect bifurcations which in turn can be followed in a two-parameter space. Similarly, when following a (e.g. Hopf) bifurcation branch, higher-order singularity bifurcation points (such as double Hopf points) can be detected. If the latter correspond to intersections of different bifurcation branches, branch switching allows to compute the intersecting branch.

Using the numerical techniques described in section 4.1 we computed the rightmost roots of the characteristic equation of the unique steady state solution of (3) along some sample one-parameter sections. In figure 2 we show the real parts of these roots for α fixed at 0.7 and $\tau_1 \in [0, 300]$. Figure 3 depicts the imaginary part of the rightmost root shown in figure 2. Figures 4 and 5 show the same for $\tau_1 = 65$ and $\alpha \in [0, 1]$. By following the Hopf bifurcations thus found figure 2 is easily reproduced numerically.

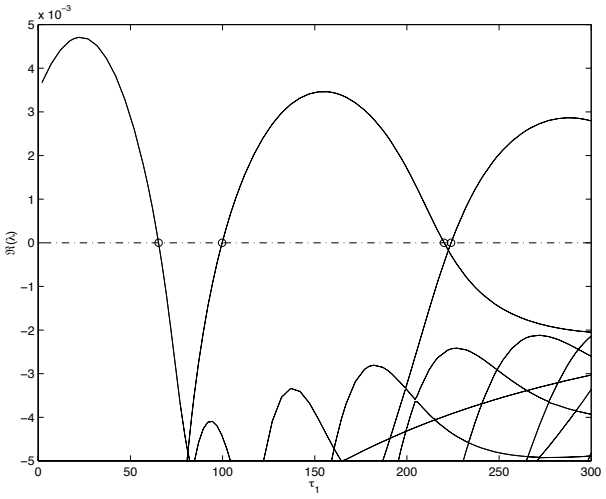

Fig. 2 The real parts of the rightmost roots of the characteristic equation of (3) along the constant solution branch (I^*, G^*) for $\alpha = 0.7$ and varying $\tau_1 \in [0, 300]$. All calculated roots consist of complex pairs, Hopf bifurcations are indicated with a 'o'.

5 Periodic Solutions

A periodic solution $z(t)$ with period $T > 0$ of (4) satisfies $z(t+T) = z(t)$, for all t. The linearization of (4) around $z(t)$ is a linear, time-

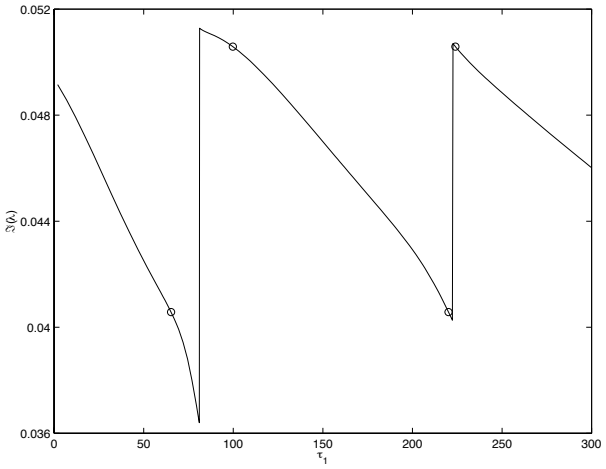

Fig. 3 The imaginary part of the rightmost root of the characteristic equation of (3) along the solution branch (I^*, G^*) for $\alpha = 0.7$ and varying $\tau_1 \in [0, 300]$. The positions of the Hopf bifurcations are indicated with a 'o'.

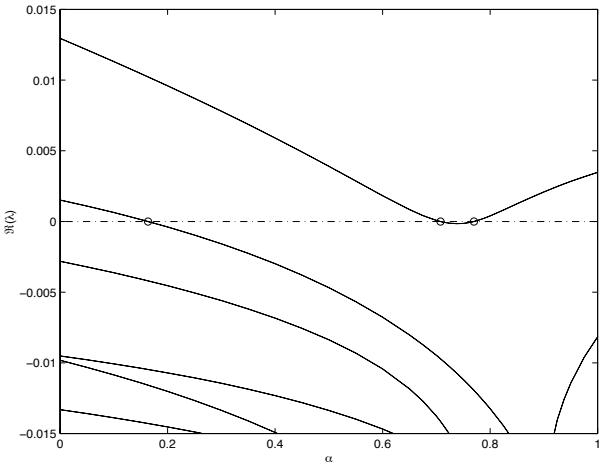

Fig. 4 The real parts of the rightmost roots of the characteristic equation of (3) along the constant solution branch (I^*, G^*) for $\tau_1 = 65$ and varying $\alpha \in [0, 1]$. All calculated roots consist of complex pairs, Hopf bifurcations are indicated with a 'o'.

dependent delay differential equation, called the variational equation of the periodic solution,

$$\dot{y}(t) = A_0(t, \eta)y(t) + \sum_{i=1}^{m} A_i(t, \eta)y(t - \tau_i), \tag{17}$$

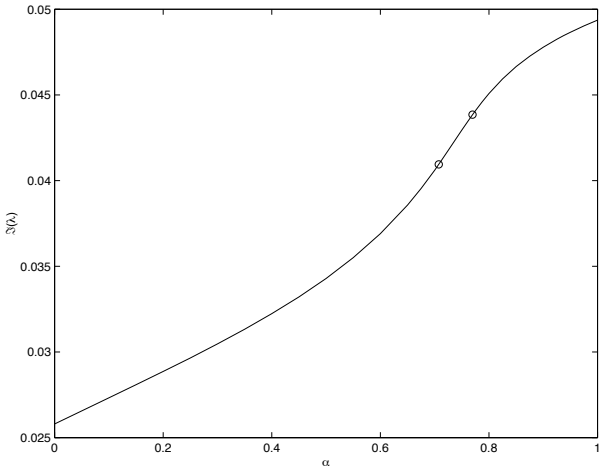

Fig. 5 The imaginary part of the rightmost root of the characteristic equation of (3) along the constant solution branch (I^*, G^*) for $\tau_1 = 65$ and varying $\alpha \in [0, 1]$. The positions of the Hopf bifurcations are indicated with a 'o'.

where the $A_i(t, \eta)$ are defined as (using again $f \equiv f(x^0, \ldots, x^m, \eta)$)

$$A_i(t, \eta) = \frac{\partial f}{\partial x^i}(z(t), z(t - \tau_1), \ldots, z(t - \tau_m), \eta), \; i = 0, \ldots, m.$$

The monodromy operator $\mathcal{S}(t_0, T)$ of the periodic solution is the operator which integrates an initial perturbation at time t_0 under the variational equation (17) over an interval of length T. Its (infinite number of) eigenvalues are called the Floquet multipliers and determine the stability of the periodic solution. Because (4) is autonomous there is always a 'trivial' Floquet multiplier equal to one which corresponds to a phase-shift along the periodic solution. The periodic solution is stable if all other Floquet multipliers have modulus smaller than one. It is unstable if there exists a Floquet multiplier with modulus greater than one.

When following a branch of periodic solutions as function of a parameter, a bifurcation occurs when a Floquet multiplier crosses through the unit circle in the complex plane. Generically, this is a period doubling bifurcation when a multiplier crosses through -1, a torus bifurcation when a pair of complex multipliers cross through the unit circle and a fold or turning point when a multiplier crosses through 1.

5.1 Numerical Methods

The periodic solutions reported in this paper are computed with a shooting based method, which we briefly explain below. A collocation based method to compute periodic solutions of delay differential equations is explained in [4].

A periodic solution, uniquely determined by an initial function segment $z_0 \in C([-\tau,0],\mathbb{R}^n)$ and the period $T>0$, can be found as the solution of a nonlinear operator equation,

$$\begin{cases} r(z_0,T) := \mathcal{S}_f(T;z_0) - z_0 = 0, \\ s(z_0,T) = 0, \end{cases} \tag{18}$$

where $\mathcal{S}_f(T,z_0)$ is the nonlinear time integration operator of the original equation (4) which integrates the initial condition z_0 over an interval of length T and $s(z_0,T)=0$ is a suitable phase condition needed to remove the translational invariancy.

Equation (18) can be solved iteratively using a Newton iteration,

$$\left[\begin{array}{cc} \frac{\partial \mathcal{S}_f(T;z_0)}{\partial z_0} - I & \frac{\partial \mathcal{S}_f(T;z_0)}{\partial T} \\ \frac{\partial s}{\partial z_0} & \frac{\partial s}{\partial T} \end{array}\right]\Bigg|_{(z_0^{(k)},T^{(k)})} \left[\begin{array}{c} \Delta z_0^{(k)} \\ \Delta T^{(k)} \end{array}\right] = - \left[\begin{array}{c} r \\ s \end{array}\right]\Bigg|_{(z_0^{(k)},T^{(k)})}, \tag{19}$$

$$z_0^{(k+1)} = z_0^{(k)} + \Delta z_0^{(k)},\ T^{(k+1)} = T^{(k)} + \Delta T^{(k)}.$$

The Fréchet derivative of $\mathcal{S}_f$, $\frac{\partial \mathcal{S}_f(T;z_0)}{\partial z_0}$, is the solution operator of the variational equation (17) around the current approximation $z^{(k)}(t)$.

We can discretize operator equation (19) by representing the function segment z_0 by its value on a discrete set of L mesh points. Let $\phi \in \mathbb{R}^N$, $N = n \times L$, be the discrete representation of the function segment z_0. The operator $\frac{\partial S_f(T;z_0)}{\partial z_0}$ can be approximated by an $N \times N$-matrix $M(T)$ with

$$M(T) = \text{Discretize}\left(\frac{\partial S_f(T;\text{Interpolate}(\phi))}{\partial \phi}\text{Interpolate}(\cdot)\right).$$

Thus, after discretization, (19) is approximated by a high-dimensional system (involving a non-sparse matrix) of the form

$$\left[\begin{array}{cc} M(T)-I & g \\ c^T & d \end{array}\right]\Bigg|_{(\phi^{(k)},T^{(k)})} \left[\begin{array}{c} \Delta\phi^{(k)} \\ \Delta T^{(k)} \end{array}\right] = - \left[\begin{array}{c} r \\ s \end{array}\right]\Bigg|_{(\phi^{(k)},T^{(k)})}, \tag{20}$$

When the Newton iteration has converged, $M(T)$ is an approximation of the monodromy operator and we call it the *monodromy matrix*. Its eigenvalues approximate the Floquet multipliers. As a consequence

$M(T)$ has an eigenvalue which approximates the trivial Floquet multiplier at 1. Its distance to 1 is, during computations, a first check of the accuracy achieved.

Solving (20) leads to an expensive method for computing periodic solutions. Not only is $M(T)^{(k)}$ a high-dimensional dense matrix whose factorization is costly, it is also expensive to construct. Indeed $M(T)^{(k)}$ is not known explicitly, instead it is defined as the discretization of a linear operator. Hence each of its columns can be found by calculating its action on a unit vector. The construction of $M(T)^{(k)}$ thus requires N time integrations of the variational equation (17), which is expensive for large N [6].

5.1.1 Newton-Picard method In [14] and the earlier references [13, 12] the Newton-Picard scheme is introduced to reduce the high cost of constructing $M(T)^{(k)}$ by exploiting its spectral properties. Let μ_i denote the i-th largest eigenvalue of $M(T)^{(k)}$ and let p be the number of eigenvalues greater than a threshold $\rho < 1$, i.e.,

$$|\mu_1| \geq |\mu_2| \geq \ldots \geq |\mu_p| > \rho > |\mu_{p+1}| \geq \ldots \geq |\mu_N|.$$

$M(T)^{(k)}$ is the discretization of a compact operator (when $T \geq \tau$) whose eigenvalues have zero as their only cluster point. Hence, we expect few large eigenvalues. This justifies the assumption that $p \ll N$. We will see in section 5.2 that this is observed in practice. In fact, one could argue that when this assumption is violated, the discretisation is too coarse for accurate bifurcation analysis.

Let the columns of $V_p \in \mathbb{R}^{N\times p}$ form an orthonormal basis for the eigenspace of $M(T)^{(k)}$ corresponding to the eigenvalues $\mu_1, \ldots, \mu_p$. Let the columns of $V_q \in \mathbb{R}^{N\times(N-p)}$ form an orthonormal basis for the orthogonal complement of this space. We now project system (20) and the unknown $\Delta\phi$ onto these two subspaces. Using the orthogonal projectors $V_pV_p^T$ and $V_qV_q^T$, $\Delta\phi$ can be decomposed as $\Delta\phi = V_q(V_q^T\Delta\phi) + V_p(V_p^T\Delta\phi)$ and the projected system is

$$\begin{bmatrix} V_q^T(M(T)-I)V_q & V_q^TM(T)V_p & V_q^Tg \\ V_p^TM(T)V_q & V_p^T(M(T)-I)V_p & V_p^Tg \\ c^TV_q & c^TV_p & d \end{bmatrix} \begin{bmatrix} V_q^T\Delta\phi \\ V_p^T\Delta\phi \\ \Delta T \end{bmatrix} = - \begin{bmatrix} V_q^Tr \\ V_p^Tr \\ s \end{bmatrix} \tag{21}$$

where, for notational convenience, we dropped the superscript which denotes the Newton-step

Because V_p is a basis for an invariant subspace of $M(T)$ and V_q is orthogonal to V_p we have $V_q^TM(T)V_p = 0$. Because at the periodic

solution g corresponds to the eigenvector of the trivial Floquet multiplier, g converges to the space spanned by V_p and we set $V_q^T g = 0$. System (21) is now partially decoupled, i.e., we can first solve the large, $(N-p)\times(N-p)$-system

$$V_q^T(M(T)-I)V_q(V_q^T\Delta\phi) = -V_q^T r, \tag{22}$$

and, then, using its solution, solve the small $p \times p$-system

$$\begin{bmatrix} V_p^T(M(T)-I)V_p & V_p^T g \\ c^T V_p & d \end{bmatrix} \begin{bmatrix} V_p^T\Delta\phi \\ \Delta T \end{bmatrix} = - \begin{bmatrix} V_p^T r \\ s \end{bmatrix} - \begin{bmatrix} V_p^T M(T) V_q \\ c^T V_q \end{bmatrix} V_q^T\Delta\phi. \tag{23}$$

Because of the construction of V_p and V_q, the spectral radius of the matrix of $V_q^T M(T)V_q$ satisfies $\sigma(V_q^T M(T)V_q) = |\mu_{p+1}| < \rho < 1$. Hence (22) can be solved iteratively with a Picard iteration. To avoid the construction of the large basis $V_q \in \mathbb{R}^{(N-p)\times(N-p)}$ this iteration can be performed in the original N-dimensional space which results in,

$$\Delta\phi_q^{[0]} = 0,\ \Delta\phi_q^{[i+1]} = QM(T)Q\Delta\phi_q^{[i]} + Qr,\ i = 0,\ldots,\nu-1, \tag{24}$$

where a projection with $Q = V_q V_q^T = I - V_p V_p^T$ is performed using only the small basis V_p; and where

$$\Delta\phi_q^{[\nu]} \approx Q\Delta\phi.$$

Using this solution of (22), the small $p\times p$-system (23) can be solved for $(V_p^T\Delta\phi, \Delta T)$ with a direct method like Gauss elimination with partial pivoting. The correction $\Delta\phi$ is now found by combining the result of the Picard iteration (24) and the solution of the reduced Newton equation (23),

$$\Delta\phi \approx \Delta\phi_q^{[\nu]} + V_p\,(V_p^T\phi),$$

hence the name Newton-Picard method.

5.1.2 Convergence and computational costs In [12] it is shown that the convergence of the Newton-Picard iteration is dominated by the Picard iteration, which has asymptotic linear convergence with convergence factor

$$|\mu_{p+1}| < \rho < 1.$$

The total cost for computing a periodic solution is determined by the total number of iterations and the work in each iteration step.

Each Newton-Picard iteration consists of three parts: computation of the invariant basis V_p of $M(T)$, the Picard iteration (24), and

the construction of the reduced Newton equation (23). The dominant cost, in each part, is the time integrations required (either as matrix-vector products with $M(T)$ or via integration of the original equations).

Computing the dominant invariant subspace of $M(T)$ can be done iteratively using subspace iteration with projection as discussed in section 4.1. Each step of subspace iteration requires p_e matrix-vector products with $M(T)$ (where p_e is slightly larger than p, e.g. $p_e = p + 4$). Except for the first iteration, we can use the subspace calculated in the previous iteration as a starting value and n_s, the number of subspace iterations required in each step, commonly equals 1 or 2.

The Picard iteration (24) requires the calculation of the residual and $\nu - 1$ matrix-vector products with $M(T)$. Constructing system (23) further requires one matrix-vector product with $M(T)$ for the right hand side. The factor $M(T)V_p$ can be recovered from the last subspace iteration.

Summing up, we conclude that the dominant cost of each iteration equals $n_s \times p_e + \nu + 1$ time integrations. Note that this number does not depend on the number of discretisation points $N = n \times L$.

5.1.3 Continuation and bifurcation analysis When following a branch of periodic solutions as function of a physical parameter $\eta \in \mathbb{R}$, the shooting method can be used as a corrector in a predictor-corrector continuation algorithm. Starting values $\phi^{(0)}$ and $T^{(0)}$ are then predicted from the previously computed branch points. Continuation can be started from a Hopf point or a stable periodic solution found using simulation.

The subspace iteration inside the Newton-Picard method yields approximations for both a basis of the dominant invariant subspace of $M(T)$ and the corresponding eigenvalues. When the iteration has converged these eigenvalues are approximations of the dominant Floquet multipliers (i.e. the Floquet multipliers larger in modulus than the threshold $\rho < 1$). Thus the computation of the relevant stability information is a natural by-product of the method and bifurcations of the computed solution can easily be detected.

When the threshold ρ is fixed, one has to allow the size p of the basis V_p to change. Indeed, new modes can come up during continuation and old modes can go away. This is one of the reasons to use $p_e - p$ extra vectors in the subspace iteration. If the eigenvalues corresponding to these extra modes have modulus greater than ρ, the subspace size p is increased. Likewise, when the eigenvalues corresponding to modes in V_p have modulus smaller than ρ, the subspace size p is decreased.

5.2 Results

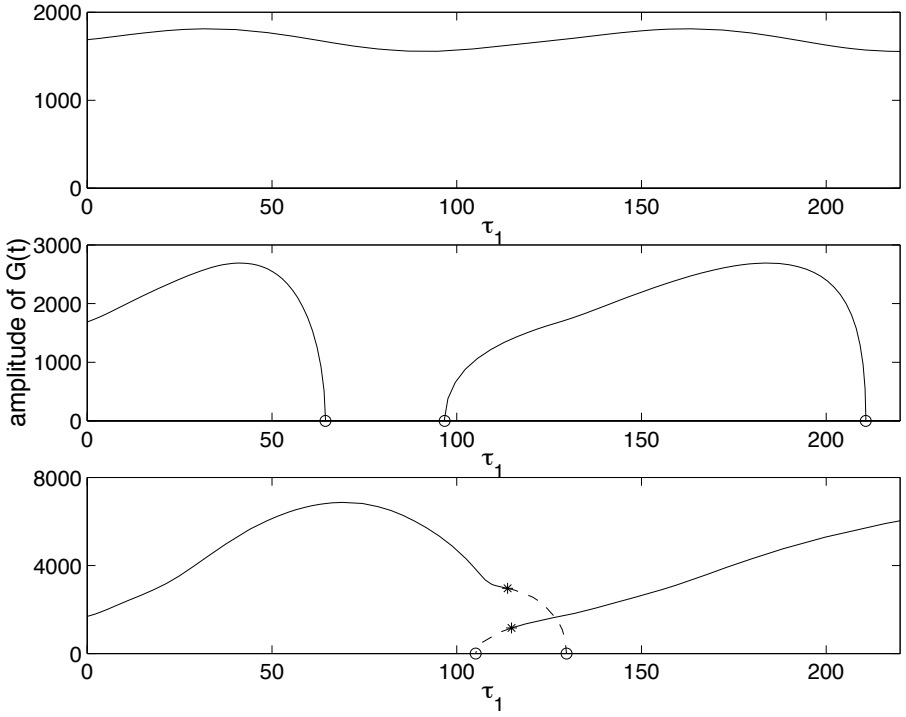

Fig. 6 The amplitude of $G(t)$ (the maximal minus the minimal value of $G(t)$, $0 \leq t \leq T$) for several branches of periodic solutions along the one-parameter sections $\alpha = 0.95$ (top), $\alpha = 0.75$ (middle) and $\alpha = 0.5$ (bottom) for varying $\tau_1 \in [0, 220]$. Stable parts are indicated with solid lines, unstable parts with dashed lines. Several Hopf bifurcations ($\circ$) and two torus bifurcations ($*$) are visible.

Branches of periodic solutions can be computed as a function of different parameters starting from the Hopf bifurcation points computed in section 4.3. This allows to investigate the direction of the bifurcating branches and to monitor their stability. As branches can turn or one can start from different Hopf points, it is possible to find stable coexisting solutions which might be missed using only simulation of the given equations. By comparing consecutive parameter sections one can investigate how the qualitative behaviour changes in a two-parameter space. We now show some typical results obtained with the method described above.

Figure 6 shows the amplitude of $G(t)$ along several branches of periodic solutions starting from and connecting Hopf points previ-

ously found. Note that for $\alpha = 1$, the external system and thus also the dependency on τ_1 disappear from system (3). Hence, at $\alpha = 1$ there is a constant solution branch as a function of τ_1 whose solutions all equal the periodic solution of a healthy patient. The branch of solutions at $\alpha = 0.95$ has a qualitatively similar behaviour. More drastic differences occur for smaller values of α (notice the different scales).

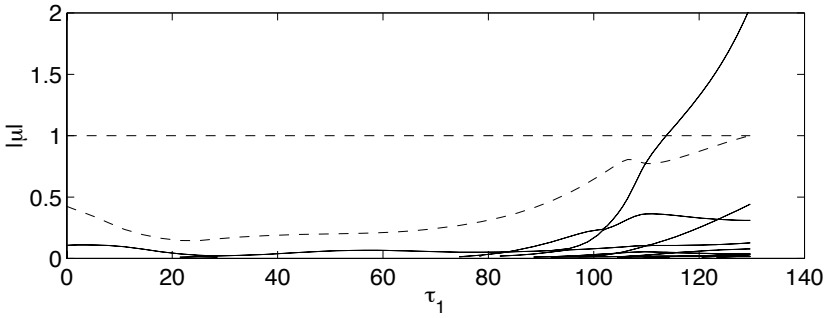

Fig. 7 The modulus of the dominant Floquet multipliers (real (− −) or complex pairs (—)) along the branch of periodic solutions shown in figure 6 (bottom, left) for $\alpha = 0.5$.

The stability along a computed branch is deduced from a computation of the dominant Floquet multipliers as depicted in figure 7. In between the two torus bifurcations shown in figure 6 (bottom) is a tiny parameter region where we did not find any stable steady state or periodic solutions. As shown in figure 8 this region grows as α decreases.

The isolated branch of periodic solutions shown in figure 8 was found using continuation in α as shown in figure 9. This branch has four unstable modes when it emanates from a Hopf bifurcation for large α. As α decreases a complex pair of Floquet multipliers enters the unit circle at a torus bifurcation. Then a real Floquet multiplier enters the unit circle at a turning point, a scenario which is repeated at a second turning point. After the second turning point the branch is stable. The intersections visible in figure 9 are a consequence of the projection on the (α, T)-plane; in the infinite-dimensional state space this branch does not self-intersect.

Figure 10 shows a phase space projection on $(G(t), I(t))$ of two coexisting stable periodic solutions for $\alpha = 0.42$ and $\tau_1 = 280$.

Some information about the computational cost and the achieved accuracy are gathered in table 1, for five consecutive continuation

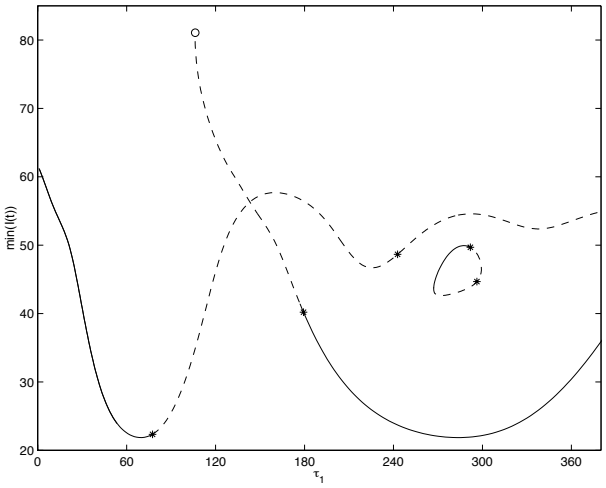

Fig. 8 Coexisting branches of periodic solutions. The minimal value of $I(t)$, $0 \leq t \leq T$ along branches of stable (—) respectively unstable (– –) periodic solutions for $\alpha = 0.42$. Two turning points, five torus bifurcations (*) and one Hopf bifurcation (o) are visible.

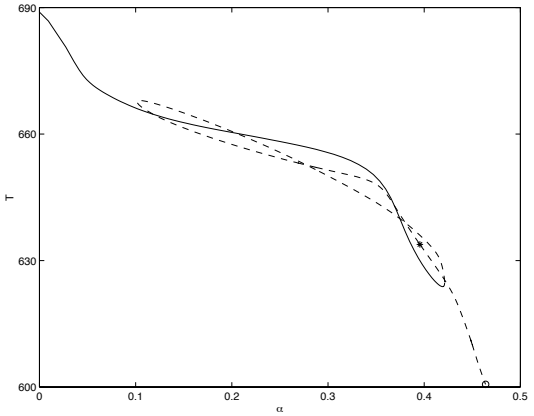

Fig. 9 The period along a branch of stable (—) respectively unstable (– –) periodic solutions for $\tau_1 \approx 283.3$. The branch starts in a Hopf bifurcation (o) at $\alpha \approx 0.46$, undergoes a torus bifurcation (*) at $\alpha \approx 0.40$ and two turning points ($\alpha \approx 0.10$, $\alpha \approx 0.42$).

points along a branch. Note that for the first point a larger number of subspace iterations is required because no initial approximation for the basis V_p is available. During these first iterations the subspace grows automatically until the final basis size is 10. For the other

points, the algorithm exploits the available data from the previously computed solution.

point number	1	2	3	4	5
Newton-Picard iterations	5	4	4	4	4
subspace iterations	14	6	7	6	6
basis size p	10	10	10	10	10
initial error $\|\|\mathcal{S}_f(T^{(0)},\phi^{(0)})-\phi^{(0)}\|\|/\|\|\phi^{(0)}\|\|$	1e-3	4e-4	3e-5	6e-5	1e-4
final error $\|\|\mathcal{S}_f(T^*,\phi^*)-\phi^*\|\|/\|\|\phi^*\|\|$	5e-16	5e-16	3e-16	3e-16	6e-16
time integrations	125	85	95	85	85

Table 1 For the first 5 computed points of a branch of periodic solutions discretized using $N = 200$ discretisation points: number of Newton-Picard iterations, number of subspace iterations, basis size p, initial and final error and total number of time integrations needed.

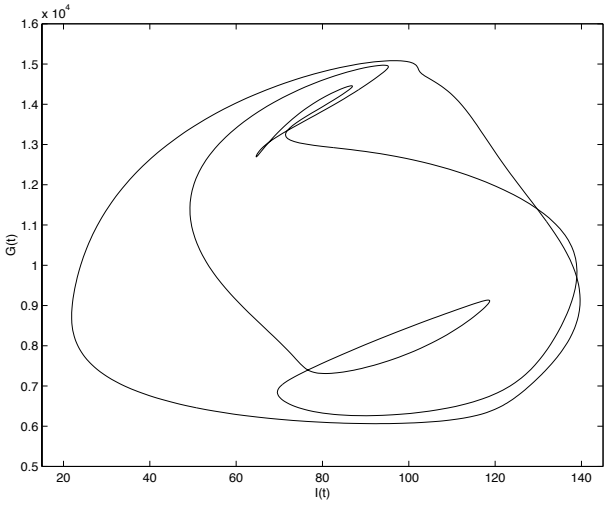

Fig. 10 Coexisting stable periodic solutions for $\alpha = 0.42$ and $\tau_1 = 280$.

In our tests we used $L = 50$ respectively $L = 100$ grid points to represent the delay segment. The first one was found sufficient to reproduce the dynamics, the second to obtain accurate positions of bifurcation points. A fine grid was needed because in this application the delay is large compared to the natural time scale of the system. The cost of the our shooting method, expressed as total number of time integrations, is independent of the number of grid points L used. Table 2 gives the expected costs of a full Newton iteration scheme.

Comparing tables 1 and 2 we can conclude that the Newton-Picard approach considerably reduces the computational costs, even for reasonable values of L and n.

n	L	N	M(T)	n_{IVP}(1 FNI)	n_{IVP}(2 FNI)
2	50	100	100×100	200	300
2	100	200	200×200	400	800

Table 2 Cost of full Newton iterations: number of delay equations n, number of grid points L, size of N, size of the monodromy matrix $M(T)$, number of time integrations required for one full Newton iteration (n_{IVP}(1 FNI)) and for two full Newton iterations (n_{IVP}(2 FNI)).

6 Physiological and Medical Implications

We now interpret the results of our analysis of model (3) to study the efficiency of external systems for glycaemia regulation. We show how, by using the numerical results presented so far, interesting medical consequences can be derived. In particular, we show that the external system is unable to restore normal glycaemia. We also show how our numerical results can help design a therapeutic intervention.

Typically, external regulation systems have a total reaction time τ_1 between 10 and 40 minutes. To evaluate the efficiency of these systems, we look at the stable solution of system (3) when $10 \leq \tau_1 \leq 40$ and $0 \leq \alpha \leq 1$, and compare it with the stable solutions of system (3) corresponding to a healthy subject (i.e. when $\tau_1 = 0$ or $\alpha = 1$). We then examine whether the difference in those profiles can be harmful to the patient, as chronic, abnormal glycaemia often leads to secondary complications of diabetes.

We thus compare the period and profile of the corresponding periodic solutions, along with their stability properties, as measured by the Floquet multipliers. In figure 6, when τ_1 has a value between 10 and 40 minutes, we note that the amplitude of $G(t)$ (as well as the amplitude of $I(t)$ in figure 11 (top)) of the corresponding periodic solution are greater than those of the reference solution ($\tau_1 = 0$). This means that we can find, in the blood and during one cycle, a higher glucose concentration and, at the same time, a higher insulin concentration than in a healthy subject. Also, it can be seen in figure 11 (bottom) that the period of the periodic solution increases noticeably when τ_1 increases. With these conditions, the external glycaemia regulation is obviously not so efficient, since the normal

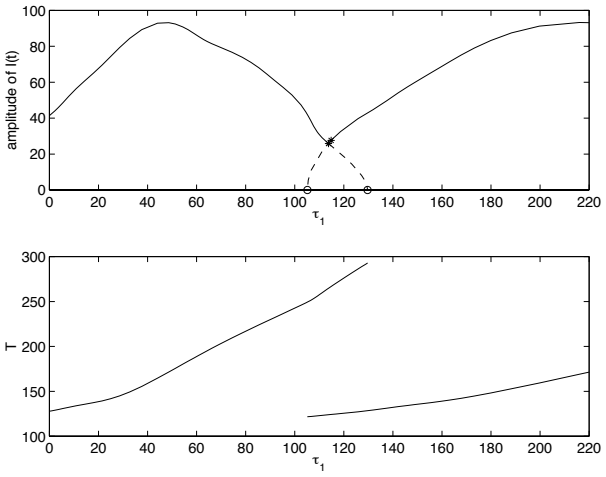

Fig. 11 The period T and the amplitude of $I(t)$ (the maximal minus the minimal value of $I(t)$, $0 \leq t \leq T$) along a branch of periodic solution for $\alpha = 0.5$ and varying $\tau_1 \in [0, 220]$.

profile and that of diabetic may differ by as much as 20% with respect to periodicity and by more than 100% with respect to amplitude. Moreover, these differences in concentration increase markedly when α takes smaller values (i.e. when considering a more affected patient).

There is nevertheless something worth observing. If we let T_0 be the period of the periodic solution when $\tau_1 = 0$, then, when system (3) is evaluated on the periodic solution we have $G(t + kT_0) = G(t)$, for all $k \in \mathbb{Z}$. Thus, in particular, $G(t - T_0) = G(t)$ and $f_1(G(t)) = f_1(G(t - \tau_1))$ for $\tau_1 = T_0$. This means that the periodic solution for $\tau_1 = 0$ has exactly the same profile as the one for $\tau_1 = T_0$ (as can be seen in figure 6 for different values of α). Hence we can increase τ_1 artificially up to $T_0 \approx 127.85$ min in order to achieve a "healthy" solution by means of the external system. But, although the profile is the same, the stability may be different because, when the system is perturbed from the periodic solution, $f_1(G(t))$ no longer equals $f_1(G(t - \tau_1))$. So, our observation remains true only as long as the periodic solution for $\tau_1 = T_0$ has the same stability as the reference solution.

What can our numerical results tell us about the stability of the periodic solution at $\tau_1 = T_0$ when α varies? Figure 12 shows the modulus of the dominant Floquet multipliers over the branch of periodic solutions with $\tau_1 = T_0 \approx 127.85$. As described above, all these solutions are identical to the periodic solution at $\tau_1 = 0$ which is the

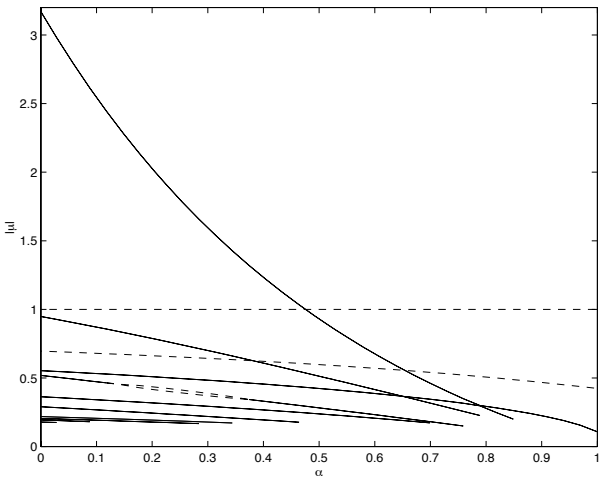

Fig. 12 The modulus of the dominant Floquet multipliers (real (– –) or complex pairs (—)) over a branch of periodic solutions for $\tau_1 = T_0 \approx 127.85$.

solution corresponding to a healthy subject. The stability however is lost through a torus bifurcation at $\alpha \approx 0.475$. (Compare with figure 8, where, at $\alpha = 0.42 < 0.475$ and $\tau_1 \approx 127.85$, there is no stable periodic solution.) The model thus indicates that there are at least two types of patients. Those for which the external system cannot bring the glycaemia to normal values (corresponding to α less than 0.475): for these patients, the reaction time τ_1 renders the external system inefficient. For the other category of patients (for which α is greater than 0.475), the external system can be made to bring, after proper tuning of τ_1, the glycaemia in a normal range. This dichotomy between two types of patients predicted by the model is reminiscent of the difference made in the medical literature between type I and type II diabetes.

The validity of the preceding remark (on choosing τ_1 equal to T_0) is further limited by our modeling hypotheses. First of all, we have to be able to model the external system with the term $(1-\alpha)f_1(G(t-\tau_1))$; this means we must be able to construct f_1 and to measure α. Then, the term which represents food intake (i.e. Eg) should not depend on time, otherwise the system would become non-autonomous. Still, we believe the insight gained is an interesting starting point which might, e.g., be complemented by a sensivity analysis to the assumptions made.

7 Conclusion

In this paper, we have described a number of numerical methods for the continuation and bifurcation analysis of steady state solutions and periodic solutions of systems of delay differential equations with an arbitrary number of fixed, discrete delays.

These algorithms have been used to analyze a mathematical model for the evolution of the blood-glucose and insulin concentration in a diabetic patient subject to a system of external assistance. This model consists of a set of two differential equations with two delays. We analyzed the local stability of its unique steady state solution and compared our numerical results with analytical ones. Whenever the steady state solution undergoes a Hopf bifurcation, an emanating branch of periodic solutions exists. We computed several branches of both stable and unstable periodic solutions and monitored their stability as determined by the dominant Floquet multipliers. We showed the occurrence of a number of bifurcations and illustrate the cost-effectiveness of our approach. The numerical analysis of the model allows us to infer the existence of two categories of patients. Those for which the external system is globally inefficient, and those, less severely affected, for which the external system need to be fine-tuned to restore normal levels of glycaemia.

Although our analysis should be complemented with an investigation of the sensitivity to the assumptions made, the results clearly give insight into the dynamical behaviour of the modeling equations. We believe a combination of analytical and numerical methods can be very useful to investigate and direct the modeling and control of physiological problems.

References

1. J. S. Christiansen, P. A. Svendsen, U. Soegaard, M. Frandsen, and E. Mathiesen. An artificial beta cell: assessment of the glucose analyser, infusion system and optimization of constants for the algorythms. *Scandanivian Journal of Clinical Laboratory Investigation*, 41:647–654, 1981.
2. E. J. Doedel, A. R. Champneys, T. F. Fairgrieve, Y. A. Kuznetsov, B. Sandstede, and X. Wang. 1997. AUTO97: Continuation and bifurcation software for ordinary differential equations; available by FTP from ftp.cs.concordia.ca in directory pub/doedel/auto.
3. K. Engelborghs. DDE-BIFTOOL: a Matlab package for bifurcation analysis of delay differential equations. Technical Report TW-305, Department of Computer Science, K.U.Leuven, Leuven, Belgium, 2000. Available from http://www.cs.kuleuven.ac.be/~koen/delay/ddebiftool.shtml.

4. K. Engelborghs, T. Luzyanina, K. J. in ′t Hout, and D. Roose. Collocation methods for the computation of periodic solutions of delay differential equations. *SIAM J. Sci. Comput.*, 2000. Accepted.
5. K. Engelborghs and D. Roose. Numerical computation of stability and detection of Hopf bifurcations of steady state solutions of delay differential equations. *Adv. Comput. Math.*, 10(3–4):271–289, 1999.
6. K. P. Hadeler. Effective computation of periodic orbits and bifurcation diagrams in delay equations. *Numerische Mathematik*, 34:457–467, 1980.
7. J. K. Hale and S. M. Verduyn Lunel. *Introduction to functional differential equations*, volume 99 of *Applied Mathematical Sciences*. Springer-Verlag, 1993.
8. B. D. Hassard, N. D. Kazarinoff, and Y-H. Wan. *Theory and applications of Hopf bifurcation*, volume 41 of *London Mathematical Society Lecture Note Series*. Cambridge University Press, 1981.
9. L. Heinemann and F. J. Ampudia-Blasco. Glucose clamps with the Biostator: a critical reappraisal. *Horm. Metab. Res.*, 26:579–583, 1994.
10. K. D. Hepp, R. Renner, H. Mehnert, and M. Franetzki. Perfusions continues d'insuline sous-cutanées et intraveineuses avec débits prédéderminés ou autoadjustés. *Journ. Ann. Diabét. Hotel*, pages 23–33, 1980.
11. A. J. Lokta. Contributions to the analysis of malaria epidemiology: I general part. *Supplement to American Journal Hygiene*, 3:1–37, 1923. (Reprinted in Scudo and Ziegler, 1978).
12. K. Lust. *Numerical bifurcation analysis of periodic solutions of partial differential equations*. PhD thesis, Katholieke Universiteit Leuven, 1997.
13. K. Lust, D. Roose, A. Spence, and A.R. Champneys. An adaptive Newton-Picard algorithm with subspace iteration for computing periodic solutions. *SIAM Journal on Scientific Computing*, 19(4):1188–1209, 1998.
14. T. Luzyanina, K. Engelborghs, K. Lust, and D. Roose. Computation, continuation and bifurcation analysis of periodic solutions of delay differential equations. *International Journal of Bifurcation and Chaos*, 7(11):2547–2560, November 1997.
15. T. Luzyanina and D. Roose. Numerical stability analysis and computation of Hopf bifurcation points for delay differential equations. *Journal of Computational and Applied Mathematics*, 72:379–392, 1996.
16. N. MacDonald. *Biological delay systems: linear stability theory*. Cambridge University Press, 1989.
17. K. Meerbergen and D. Roose. Matrix transformations for computing rightmost eigenvalues of large sparse non-symmetric eigenvalue problems. *IMA Journal of Numerical Analysis*, 16:297–346, 1996.
18. J. Mirouze, J. L. Selam, T. C. Pham, and D. Cavadore. Evaluation of exogenous insulin homeostasis by the artificial pancreas in insulin-dependent diabetes. *Diabetologia*, 13:273–278, 1977.
19. A. H. Nayfeh and B. Balachandran. *Applied nonlinear dynamics*. Wiley Series in Nonlinear Science. Wiley-Interscience Publication, 1995.
20. E. F. Pfeiffer, C. Thum, and A. H. Clemens. The artificial beta cell – a continuous control of blood sugar by external regulation of insulin. *Horm. Metab. Res.*, 487:339–342, 1974.
21. J. Pickup. Developing glucose sensors for in vivo use. *TIBTech*, 11:285–291, 1993.
22. Youcef Saad. *Numerical Methods for Large Eigenvalue Problems*. Manchester University Press, 1992.

23. J. V. Santiago, A. H. Clemens, W. L. Clarke, and D. M. Kipnis. Closed-loop and open-loop devices for blood glucose control in normal and diabetic subjects. *Diabetes*, 28(1):71–81, 1979.
24. G. Slama and J. L. Selam. Pompes à insuline externes et implantables et autres techniques d'insulinothérapie. *Journ. Ann. Diabét. Hotel*, pages 111–122, 1992.
25. J Sturis, K. S. Polonsky, E. Mosekilde, and E. Van Cauter. Computer model for mechanisms underlying ultradian oscillations of insulin and glucose. *Am. J. Physiol.*, 260:E801–E809, 1991.
26. V. Volterra. Variazioni et fluttuazioni del numero d'individui in specie animali conviventi. *R. Comitato Talassografico Memoria*, 131:1–142, 1927. (Translation appears in Scudo and Ziegler, 1978).

Acknowledgements This research presents results of the research project OT/98/16, funded by the Research Council K.U.Leuven and of the research project IUAP P4/02 funded by the programme on Interuniversity Poles of Attraction, initiated by the Belgian State, Prime Minister's Office for Science, Technology and Culture. K. Engelborghs is a Research Assistant of the Fund for Scientific Research - Flanders (Belgium). This work was supported by grants from Natural Sciences and Engineering Research Council (Canada) and Fonds de Chercheurs et d'Aide a la Recherche (Quebec) to J. Bélair.

We thank the referees for their suggestions which lead to an improved final version of the manuscript.